PROCEEDINGS OF THE ROYAL SOCIETY A

FirstCite® e-publishing

Proc. R. Soc. A
doi:10.1098/rspa.2007.0016
Published online

Event-driven feedback tracking and control of tapping-mode atomic force microscopy

By Sambit Misra[1], Harry Dankowicz[1,*] and Mark R. Paul[2]

[1]*Mechanical Science and Engineering, University of Illinois at Urbana-Champaign, Urbana, IL 61801, USA*
[2]*Mechanical Engineering, Virginia Polytechnic Institute and State University, Blacksburg, VA 24061, USA*

This paper presents an event-driven, discrete-in-time feedback strategy for tracking and stabilizing naturally occurring periodic oscillations in the probe-tip dynamics of atomic force microscope (AFM) cantilevers in tapping-mode operation. Specifically, robust dynamic tracking and stabilization is achieved by the imposition of discrete changes in the vertical offset between the cantilever support and the sample surface based on an estimated linearization of the system dynamics about a dynamically generated reference trajectory. Here, use is made not only of the oscillation amplitude, as is typical in commercial control implementations for AFMs, but also of the instantaneous phase information. It is shown that stabilization and desirable performance during surface scanning is possible, even in the presence of uncertainty and limited state access. In particular, the methodology enables robust tracking and use of low-contact-velocity periodic system responses that are unstable in the absence of control.

Keywords: tapping-mode; atomic force microscopy; OGY control; stabilization

1. Introduction

In this paper, we present a collection of dynamical systems-based, control-theoretic, analytical and computational tools for investigating and exploiting the natural dynamics of the atomic force microscope (AFM) cantilever during tapping-mode operation.

AFM systems are widely used for nano-scale material characterization. In particular, tapping-mode operation is one of the more popular measurement modalities for soft and biomaterial applications. In tapping-mode AFM, vibrations of the cantilever tip are induced through oscillations of a dither piezo at the cantilever support and the output is modulated due to the presence of various attractive and repulsive forces as the tip moves in an almost periodic motion. Owing to the nonlinear tip–sample interaction forces, the cantilever response exhibits nonlinear system characteristics, such as bifurcations, coexistence of multiple solutions and chaos (García & San Paulo 2000; Lee *et al.* 2002; San Paulo & García 2002; Yagasaki 2004; Jamitzky *et al.* 2006; Zhao & Dankowicz 2006;

* Author for correspondence (danko@uiuc.edu).

Received 4 May 2007
Accepted 17 March 2008

Dankowicz *et al.* 2007). These characteristics and their impact on the imaging capability of the AFM system have motivated the use of several feedback techniques to carefully control the dynamic response of the AFM cantilever (Ashhab *et al.* 1997; Stark 2005; Uchihashi *et al.* 2006).

The introduction of feedback for controlling chaos and/or stabilizing unstable periodic oscillations is an active field of research in the nonlinear dynamics and control communities with applications ranging from electronic oscillator circuits to population dynamics (see Andreivskii & Fradkov 2003). Many of the current applications of discrete feedback control in achieving stabilization or avoiding chaos can be traced back to the seminal work by Ott *et al.* (1990). The idea behind the control strategy is to effect changes in the stability characteristics of a periodic oscillation by an event-driven imposition of discrete changes to a system state or a parameter based on some suitable feedback scheme. The changes may, for example, be chosen to be proportional to the deviation between the actual and desired states or between the actual states at two successive measurements (cf. the continuous-in-time delay feedback strategy of an AFM cantilever described in Yamasue & Hikihara (2006)). In particular, the latter strategy allows for stabilization of inaccurately known periodic oscillations and can be extended to overcome stability restrictions to allow for tracking of drifting periodic oscillations. The original version of the Ott *et al.* (1990) algorithm was described for discrete-time systems (iterated maps) of dimension two and for continuous-time systems of dimension three and required online computation of the eigenvectors and eigenvalues of a suitably defined sensitivity matrix of the desired motion. Numerous extensions and interpretations have been proposed by different authors in subsequent years and the method is now commonly referred to as the *OGY method* after the authors of the Ott *et al.* paper (see Andreivskii & Fradkov 2003).

This paper is organized as follows. In §2, a variety of OGY-based formulations are proposed for controlling the linearized stability characteristics of a periodic oscillation of a generic piecewise-smooth dynamical system, for estimating the linearized dynamics in the vicinity of a given periodic oscillation and for tracking periodic oscillations under parameter variations. Section 3 contains a model-based discussion of the AFM cantilever dynamics and a formulation of control objectives to which the theoretical formulation of §2 is subsequently applied. In particular, in §4, numerical results obtained from such an application are presented, which document increases in the speed of surface scanning, while preventing undesired transitions between different cantilever oscillations, as well as successful use of (in the absence of control) unstable cantilever oscillations that achieve tapping-mode operation with relatively small contact velocities and short duration of contact. This paper concludes with a discussion of possible avenues for further work.

2. An event-driven control strategy

The OGY control strategy provides a means for changing the linearized stability characteristics of a periodic system response by the imposition of discrete feedback control of a system parameter effected at each intersection of an actual state-space trajectory with a transversal hypersurface $\mathcal{P}$, known as a *Poincaré section*. In the discrete formulation, the stability characteristics of the

periodic system response are directly related to the stability characteristics of a fixed point of an iterated map $\boldsymbol{P}$, defined on the Poincaré section, namely the point of intersection of the corresponding closed state-space trajectory with the Poincaré section.

Denote by $\boldsymbol{x}^*$ the point of intersection of the closed state-space trajectory with $\mathcal{P}$. Here, the bold-italic characters denote elements of state space, for example the space of all n-tuplets $\mathbb{R}^n$, where n is the dimension of the dynamical system. Then, the *Poincaré map* $\boldsymbol{P}$: $\mathcal{P}\to\mathcal{P}$ maps a current point of intersection $\boldsymbol{x}\in\mathcal{P}$ to the subsequent point of intersection with $\mathcal{P}$ of the corresponding state-space trajectory. In particular, since $\boldsymbol{x}^*$ lies on a closed state-space trajectory, $\boldsymbol{P}(\boldsymbol{x}^*)=\boldsymbol{x}^*$. Under reasonable assumptions on the dynamical system, $\boldsymbol{P}$ is a smooth function of $\boldsymbol{x}$ for $\boldsymbol{x}\approx\boldsymbol{x}^*$. From *Taylor's theorem*, it follows that

$$\boldsymbol{P}(\boldsymbol{x}) \approx \boldsymbol{x}^* + \partial_{\boldsymbol{x}}\boldsymbol{P}(\boldsymbol{x}^*)\cdot(\boldsymbol{x}-\boldsymbol{x}^*), \tag{2.1}$$

for $\boldsymbol{x}\approx\boldsymbol{x}^*$, i.e. the deviation of the image of $\boldsymbol{x}$ under $\boldsymbol{P}$ from $\boldsymbol{x}^*$ is approximately linear in the deviation $\boldsymbol{x}-\boldsymbol{x}^*$. The *sensitivity matrix* $\partial_{\boldsymbol{x}}\boldsymbol{P}(\boldsymbol{x}^*)$ is known as the *Jacobian* of the Poincaré map evaluated at the fixed point $\boldsymbol{x}^*$ and consists of first partial derivatives of the components of $\boldsymbol{P}(\boldsymbol{x})$ with respect to the components of $\boldsymbol{x}$. Specifically, the (i, j)th component of the sensitivity matrix describes the rate of change of the ith component of the subsequent point of intersection with respect to the changes in the jth component of the current point of intersection.

Knowledge of the sensitivity matrix $\partial_{\boldsymbol{x}}\boldsymbol{P}(\boldsymbol{x}^*)$ and its properties provides a linearized description of the state-space dynamics near the closed state-space trajectory. For example, as long as all its *eigenvalues* (i.e. the roots to the characteristic equation

$$\det(\partial_{\boldsymbol{x}}\boldsymbol{P}(\boldsymbol{x}^*)-\lambda\mathbf{1}) = 0, \tag{2.2}$$

where $\mathbf{1}$ denotes the identity matrix) lie within the unit circle in the complex plane (i.e. have a magnitude less than 1), the fixed point $\boldsymbol{x}^*$ is *asymptotically stable in the Lyapunov sense* under iterations of $\boldsymbol{P}$. In this case, there exists a neighbourhood of points $\boldsymbol{x}\approx\boldsymbol{x}^*$, such that subsequent iterates under the action of $\boldsymbol{P}$ stay within a given distance from $\boldsymbol{x}^*$ and eventually approach $\boldsymbol{x}^*$ arbitrarily closely.

(*a*) *Full-state feedback*

Denote by p a system parameter and write $\boldsymbol{P}(\boldsymbol{x}, p)$ for the Poincaré map from a current point of intersection $\boldsymbol{x}\in\mathcal{P}$ to the subsequent point of intersection with $\mathcal{P}$ of the corresponding state-space trajectory, given a particular value for the parameter p. Suppose that $\boldsymbol{x}^*$ is a fixed point of the Poincaré map $\boldsymbol{P}$ for $p=p^*$. It again follows that

$$\boldsymbol{P}(\boldsymbol{x}, p) \approx \boldsymbol{x}^* + \partial_{\boldsymbol{x}}\boldsymbol{P}(\boldsymbol{x}^*, p^*)\cdot(\boldsymbol{x}-\boldsymbol{x}^*) + \partial_p\boldsymbol{P}(\boldsymbol{x}^*, p^*)(p-p^*), \tag{2.3}$$

for $\boldsymbol{x}\approx\boldsymbol{x}^*$ and $p\approx p^*$, where $\partial_p\boldsymbol{P}(\boldsymbol{x}^*, p^*)$ is a column matrix of first partial derivatives of the components of $\boldsymbol{P}(\boldsymbol{x}, p)$ with respect to p evaluated at $\boldsymbol{x}=\boldsymbol{x}^*$ and $p=p^*$.

Suppose that g is a smooth function of $\boldsymbol{x}$ and p for $\boldsymbol{x}\approx\boldsymbol{x}^*$ and $p\approx p^*$, such that $g(\boldsymbol{x}^*,p^*)=0$. The imposition of control as per the OGY strategy amounts to the event-driven introduction of a feedback correction

$$\boldsymbol{g}_{\text{control}} : \begin{pmatrix} \boldsymbol{x} \\ p \end{pmatrix} \mapsto \begin{pmatrix} \boldsymbol{x} \\ p + g(\boldsymbol{x}, p) \end{pmatrix}, \tag{2.4}$$

such that the Poincaré map for the controlled system is given by the composition $(\boldsymbol{P} \quad \boldsymbol{I})^{\mathrm{T}} \circ \boldsymbol{g}_{\mathrm{control}}$, where $\boldsymbol{I}$ denotes the identity map. Let $\delta\boldsymbol{x}=\boldsymbol{x}-\boldsymbol{x}^*$ denote the deviation between an arbitrary point on $\mathcal{P}$ and the fixed point $\boldsymbol{x}^*$ and $\delta p=p-p^*$ denote the deviation between a given parameter value and the parameter value corresponding to the fixed point $\boldsymbol{x}^*$. Use integer superscripts within parentheses to index a sequence of iterates of these deviations under the action of the composite Poincaré map. Taylor's theorem again implies that

$$\boldsymbol{z}^{(k+1)} \approx A\boldsymbol{z}^{(k)} + Bu^{(k)} \tag{2.5}$$

and

$$u^{(k)} = K\boldsymbol{z}^{(k)}, \tag{2.6}$$

where

$$\boldsymbol{z} = \begin{pmatrix} \delta\boldsymbol{x} \\ \delta p \end{pmatrix}, \qquad A = \begin{pmatrix} \partial_{\boldsymbol{x}}\boldsymbol{P}(\boldsymbol{x}^*, p^*) & \partial_p\boldsymbol{P}(\boldsymbol{x}^*, p^*) \\ \boldsymbol{0} & 1 \end{pmatrix}, \tag{2.7}$$

$$B = \begin{pmatrix} \partial_p\boldsymbol{P}(\boldsymbol{x}^*, p^*) \\ 1 \end{pmatrix} \quad \text{and} \quad K = \begin{pmatrix} \partial_{\boldsymbol{x}} g(\boldsymbol{x}^*, p^*) & \partial_p g(\boldsymbol{x}^*, p^*) \end{pmatrix}. \tag{2.8}$$

From the linear control theory of discrete dynamical systems (cf. Chen 1999), it follows that as long as the pair (A, B) is *controllable*, i.e. as long as

$$\operatorname{rank}\begin{pmatrix} B & AB & A^2B & \dots & A^nB \end{pmatrix} = n+1, \tag{2.9}$$

where n is the dimension of state space, the eigenvalues of the matrix $A+BK$ may be placed in any desired position by suitable choices of the entries of K. It follows that the asymptotic stability of $(\boldsymbol{x}^*, p^*)^{\mathrm{T}}$ may be ensured under the iterations of the composite Poincaré map by a suitable design of the linearization of the control map $\boldsymbol{g}_{\mathrm{control}}$ evaluated at $(\boldsymbol{x}^*, p^*)^{\mathrm{T}}$.

(*b*) *Estimated-state feedback*

In the case when the value of p is not directly available, as would be the case if the value of p was not directly measurable, it is no longer possible to place the eigenvalues arbitrarily using the above feedback strategy. Suppose that g, $\boldsymbol{h}$ and k are smooth functions of $\boldsymbol{x}$ and p and of $\boldsymbol{x}-\boldsymbol{x}^*$, respectively, for $\boldsymbol{x}\approx\boldsymbol{x}^*$ and $p\approx p^*$, such that $g(\boldsymbol{x}^*,p^*)=0$, $\boldsymbol{h}(\boldsymbol{0})=\boldsymbol{0}$ and $k(\boldsymbol{0})=0$. Consider, in this case, the event-driven introduction of a feedback correction

$$\boldsymbol{g}_{\mathrm{control}} : \begin{pmatrix} \boldsymbol{x} \\ p \\ \tilde{\boldsymbol{x}} \\ \tilde{p} \end{pmatrix} \mapsto \begin{pmatrix} \boldsymbol{x} \\ p + g(\tilde{\boldsymbol{x}}, \tilde{p}) \\ \boldsymbol{P}(\tilde{\boldsymbol{x}}, \tilde{p} + g(\tilde{\boldsymbol{x}}, \tilde{p})) + \boldsymbol{h}(\boldsymbol{x}-\tilde{\boldsymbol{x}}) \\ \tilde{p} + g(\tilde{\boldsymbol{x}}, \tilde{p}) + k(\boldsymbol{x}-\boldsymbol{x}^*) \end{pmatrix}, \tag{2.10}$$

where $\tilde{\boldsymbol{x}}$ and $\tilde{p}$ are the model-based estimated values of $\boldsymbol{x}$ and p, such that the Poincaré map for the controlled system is given by the composition

$(\boldsymbol{P} \quad \boldsymbol{I} \quad \boldsymbol{I} \quad \boldsymbol{I})^{\mathrm{T}} \circ \boldsymbol{g}_{\mathrm{control}}$. Let $\delta\tilde{\boldsymbol{x}} = \tilde{\boldsymbol{x}} - \boldsymbol{x}^*$ and $\delta\tilde{p} = \tilde{p} - p^*$. Taylor's theorem again implies

$$\boldsymbol{z}^{(k+1)} \approx A\boldsymbol{z}^{(k)} + Bu^{(k)}, \tag{2.11}$$

$$u^{(k)} = K\tilde{\boldsymbol{z}}^{(k)} \tag{2.12}$$

and

$$\tilde{\boldsymbol{z}}^{(k+1)} \approx A\tilde{\boldsymbol{z}}^{(k)} + Bu^{(k)} + LC(\boldsymbol{z}^{(k)} - \tilde{\boldsymbol{z}}^{(k)}), \tag{2.13}$$

where

$$\boldsymbol{z} = \begin{pmatrix} \delta\boldsymbol{x} \\ \delta p \end{pmatrix}, \qquad \tilde{\boldsymbol{z}} = \begin{pmatrix} \delta\tilde{\boldsymbol{x}} \\ \delta\tilde{p} \end{pmatrix}, \qquad A = \begin{pmatrix} \partial_{\boldsymbol{x}}\boldsymbol{P}(\boldsymbol{x}^*, p^*) & \partial_p\boldsymbol{P}(\boldsymbol{x}^*, p^*) \\ \boldsymbol{0} & 1 \end{pmatrix}, \tag{2.14}$$

$$B = \begin{pmatrix} \partial_p\boldsymbol{P}(\boldsymbol{x}^*, \boldsymbol{p}^*) \\ 1 \end{pmatrix}, \qquad C = (\,\boldsymbol{1} \quad 0\,), \tag{2.15}$$

$$K = \begin{pmatrix} \partial_{\boldsymbol{x}} g(\boldsymbol{x}^*, p^*) & \partial_p g(\boldsymbol{x}^*, p^*) \end{pmatrix} \quad \text{and} \quad L = \begin{pmatrix} \partial_{\boldsymbol{x}}\boldsymbol{h}(\boldsymbol{0}) \\ \partial_x k(\boldsymbol{0}) \end{pmatrix}. \tag{2.16}$$

From the linear control theory of discrete dynamical systems (cf. Chen 1999), it follows that as long as the pair (A, C) is *observable*, i.e. as long as

$$\operatorname{rank} \begin{pmatrix} C \\ CA \\ CA^2 \\ \vdots \\ CA^n \end{pmatrix}^{\mathrm{T}} = n + 1, \tag{2.17}$$

the eigenvalues of the matrix $A + LC$ may be placed in any desired position by suitable choices of the entries of L. But,

$$\begin{pmatrix} \boldsymbol{z}^{(k+1)} \\ \boldsymbol{z}^{(k+1)} - \tilde{\boldsymbol{z}}^{(k+1)} \end{pmatrix} = \begin{pmatrix} A + BK & BK \\ 0 & A + LC \end{pmatrix} \begin{pmatrix} \boldsymbol{z}^{(k)} \\ \boldsymbol{z}^{(k)} - \tilde{\boldsymbol{z}}^{(k)} \end{pmatrix}, \tag{2.18}$$

from which we conclude that asymptotic stability of $(\boldsymbol{x}^*, p^*, \boldsymbol{x}^*, p^*)$ may be ensured under the iterations of the composite Poincaré map, given the controllability of the pair (A, B) and the observability of the pair (A, C).

(*c*) *Remarks*

Remark 2.1. Although it is not generally possible to place the eigenvalues in any desired position in the case that the parameter p cannot be directly observed (Syrmos *et al.* 1997), it may still be possible, in individual cases, to design the control strategy $\boldsymbol{g}_{\mathrm{control}}$ in (2.4) so as to ensure asymptotic stability. Indeed, although $\partial_p g(\boldsymbol{x}^*, p^*) = 0$, appropriate choices of values of the components of

$\partial_{\boldsymbol{x}} g(\boldsymbol{x}^*, p^*)$ may still exist, which achieve a closed-loop system in which all eigenvalues are contained within the unit circle. Such a feedback case is henceforth referred to as the partial-state feedback (also known as *static output feedback*) strategy. In the absence of an analytical framework for locating such numerical values, numerical optimization algorithms may be employed to search parameter space corresponding to the non-zero components of K. This methodology may also be used to increase the linearized stability margins in the case of periodic oscillations that are asymptotically stable already in the absence of feedback.

Remark 2.2. The estimated-state feedback strategy described here is an example of a *Luenberger observer*. Here, stabilizability is ensured through the introduction of an *estimator*, an auxiliary discrete dynamical system with state variable $\tilde{\boldsymbol{x}}$ and parameter $\tilde{p}$ that can be made to converge to the original dynamical system and thereby provide an approximate value for $\boldsymbol{x}$ and p for use in the control map.

Remark 2.3. The arbitrary placement of the eigenvalues of the $A+BK$ matrix may require numerically large in magnitude values of the entries of K. This may be of concern in a practical implementation. Moreover, it can be shown that the robustness of the estimated-state feedback strategy in an actual application requires that one select the entries of K and L, such that the eigenvalues of $A+LC$ are smaller in magnitude than those of the $A+BK$ system.

Remark 2.4. Let $\boldsymbol{f}$ denote a smooth vector field describing the dynamical system in some region of state space. Denote by $\phi(\boldsymbol{x}, t, p)$ the system response as a function of time t, given an initial condition $\boldsymbol{x}$ and a parameter value p, i.e. such that $\phi(\boldsymbol{x}, 0, p) = \boldsymbol{x}$ and

$$\partial_t \phi(\boldsymbol{x}, t, p) = \boldsymbol{f}(\phi(\boldsymbol{x}, t, p), p). \tag{2.19}$$

It follows that $\partial_{\boldsymbol{x}} \phi(\boldsymbol{x}, 0, p) = \mathbf{1}$ and

$$\partial_t \partial_{\boldsymbol{x}} \phi(\boldsymbol{x}, t, p) = \partial_{\boldsymbol{x}} \boldsymbol{f}(\phi(\boldsymbol{x}, t, p), p) \cdot \partial_{\boldsymbol{x}} \phi(\boldsymbol{x}, t, p), \tag{2.20}$$

which is known as the *first variational equation*. The solution of the corresponding initial-value problem yields the sensitivity matrix $\partial_{\boldsymbol{x}} \phi(\boldsymbol{x}, t, p)$, describing the rate of change of the final condition along a state-space trajectory after elapsed time t with respect to the changes in the initial condition.

Now suppose that $\boldsymbol{x}^*$ is a point on a state-space trajectory segment for $p = p^*$, such that $h_{\mathcal{P}}(\boldsymbol{x}^*) = 0$ for some smooth function $h_{\mathcal{P}}$ and $\partial_{\boldsymbol{x}} h_{\mathcal{P}}(\boldsymbol{x}^*) \cdot \boldsymbol{f}(\boldsymbol{x}^*, p^*) \neq 0$, i.e. such that $\boldsymbol{x}^*$ is a point of transversal intersection of the trajectory segment with the Poincaré section $\mathcal{P}$ corresponding to the zero-level surface of $h_{\mathcal{P}}$. By the *implicit function theorem*, it follows that there exists a map $\tilde{\boldsymbol{P}}$ that maps arbitrary points near $\boldsymbol{x}^*$ to the nearest intersection with $\mathcal{P}$ of the corresponding state-space trajectories for $p \approx p^*$. In particular, $\tilde{\boldsymbol{P}}(\boldsymbol{x}^*, p^*) = \boldsymbol{x}^*$ and

$$\partial_{\boldsymbol{x}} \tilde{\boldsymbol{P}}(\boldsymbol{x}^*, p^*) = \mathbf{1} - \frac{\boldsymbol{f}(\boldsymbol{x}^*, p^*) \cdot \partial_{\boldsymbol{x}} h_{\mathcal{P}}(\boldsymbol{x}^*)}{\partial_{\boldsymbol{x}} h_{\mathcal{P}}(\boldsymbol{x}^*) \cdot \boldsymbol{f}(\boldsymbol{x}^*, p^*)}. \tag{2.21}$$

Now suppose that $\boldsymbol{x}^*$ and $\boldsymbol{x}^{**} = \phi(\boldsymbol{x}^*, T, p^*)$ are points on a state-space trajectory segment, such that $h_{\mathcal{P}_1}(\boldsymbol{x}^*) = h_{\mathcal{P}_2}(\boldsymbol{x}^{**}) = 0$ for some smooth functions $h_{\mathcal{P}_1}$ and $h_{\mathcal{P}_2}$, $\partial_{\boldsymbol{x}} h_{\mathcal{P}_2}(\boldsymbol{x}^{**}) \cdot \boldsymbol{f}(\boldsymbol{x}^{**}, p^*) \neq 0$, and such that $h_{\mathcal{P}_1}(\phi(\boldsymbol{x}^*, t, p^*)) \neq 0$, $h_{\mathcal{P}_2}(\phi(\boldsymbol{x}^*, t, p^*)) \neq 0$

for $t \in (0,\, T)$. Denote by $\hat{\boldsymbol{P}}$ the map that maps arbitrary points on $\mathcal{P}_1$ near $\boldsymbol{x}^*$ to the next intersection with $\mathcal{P}_2$ along the corresponding state-space trajectory for $p \approx p^*$. Then, $\hat{\boldsymbol{P}}(\boldsymbol{x}^*, p^*) = \boldsymbol{x}^{**}$ and

$$\partial_{\boldsymbol{x}} \hat{\boldsymbol{P}}(\boldsymbol{x}^*, p^*) = \left[\mathbf{1} - \frac{\boldsymbol{f}(\boldsymbol{x}^{**}, p^*) \cdot \partial_{\boldsymbol{x}} h_{\mathcal{P}_2}(\boldsymbol{x}^{**})}{\partial_{\boldsymbol{x}} h_{\mathcal{P}_2}(\boldsymbol{x}^{**}) \cdot \boldsymbol{f}(\boldsymbol{x}^{**}, p^*)} \right] \cdot \partial_{\boldsymbol{x}} \phi(\boldsymbol{x}^*,\, T,\, p^*). \tag{2.22}$$

In a piecewise-smooth system with only transversal intersections with state-space discontinuity surfaces, the elements of the coefficient matrix A discussed earlier can be constructed through the composition of one or more segments of the type discussed here.

Remark 2.5. Consider again the map $\boldsymbol{P}(\cdot, p)$ that maps arbitrary points near $\boldsymbol{x}^* \in \mathcal{P}$ to the nearest intersection with $\mathcal{P}$ of the corresponding state-space trajectories, given the parameter value p, and suppose that $\mathcal{P}$ is the zero-level surface of a smooth function $h_{\mathcal{P}}$. Then,

$$h_{\mathcal{P}}(\boldsymbol{P}(\boldsymbol{x}, p)) = 0, \tag{2.23}$$

for $\boldsymbol{x} \approx \boldsymbol{x}^*$ and $p \approx p^*$ implies that

$$\partial_{\boldsymbol{x}} h_{\mathcal{P}}(\boldsymbol{x}^*) \cdot \begin{pmatrix} \partial_{\boldsymbol{x}} \boldsymbol{P}(\boldsymbol{x}^*, p^*) & \partial_p \boldsymbol{P}(\boldsymbol{x}^*, p^*) \end{pmatrix} = \begin{pmatrix} \mathbf{0} & 0 \end{pmatrix}. \tag{2.24}$$

It follows that

$$\begin{pmatrix} \partial_{\boldsymbol{x}} h_{\mathcal{P}}(\boldsymbol{x}^*) & 0 \end{pmatrix} \cdot \begin{pmatrix} \partial_{\boldsymbol{x}} \boldsymbol{P}(\boldsymbol{x}^*, p^*) & \partial_p \boldsymbol{P}(\boldsymbol{x}^*, p^*) \\ 0 & 1 \end{pmatrix}^k \cdot \begin{pmatrix} \partial_p \boldsymbol{P}(\boldsymbol{x}^*, p^*) \\ 1 \end{pmatrix} = 0, \tag{2.25}$$

for all k, i.e.

$$\operatorname{rank} \begin{pmatrix} B & AB & A^2B & \dots & A^nB \end{pmatrix} \leq n. \tag{2.26}$$

On the other hand, it also follows that

$$\begin{pmatrix} \partial_{\boldsymbol{x}} h_{\mathcal{P}}(\boldsymbol{x}^*) & 0 \end{pmatrix} \cdot (A + BK) = 0, \tag{2.27}$$

for arbitrary K, i.e. 0 is an eigenvalue of $A + BK$ independently of K. The controllability criterion in this case then requires only that

$$\operatorname{rank} \begin{pmatrix} B & AB & A^2B & \dots & A^nB \end{pmatrix} = n. \tag{2.28}$$

Remark 2.6. In contrast to direct methods based on numerical integration of the differential equations governing the system dynamics, iterative methods may be employed to locate stable, as well as unstable, periodic trajectories. Consider, for example, the function

$$\boldsymbol{F}(\boldsymbol{x}, p) \stackrel{\text{def}}{=} \boldsymbol{P}(\boldsymbol{x}, p) - \boldsymbol{x}, \tag{2.29}$$

where $\boldsymbol{P}$ is the map defined above, such that

$$\boldsymbol{F}(\boldsymbol{x}^*, p^*) = \mathbf{0}. \tag{2.30}$$

Suppose that the Jacobian $\partial_{\boldsymbol{x}} \boldsymbol{P}(\boldsymbol{x}^*, p^*)$ has no eigenvalue equal to 1. It follows that the matrix

$$\partial_{\boldsymbol{x}} \boldsymbol{F}(\boldsymbol{x}^*, p^*) = \partial_{\boldsymbol{x}} \boldsymbol{P}(\boldsymbol{x}^*, p^*) - \mathbf{1}, \tag{2.31}$$

is non-singular. The implicit function theorem then implies the existence of a unique smooth function $\boldsymbol{\xi}(p)$ for $p \approx p^*$, such that $\boldsymbol{\xi}(p^*) = \boldsymbol{x}^*$,

$$\boldsymbol{F}(\boldsymbol{\xi}(p), p) \equiv \mathbf{0} \quad \text{and} \quad \partial_p \boldsymbol{\xi}(p^*) = -(\partial_x \boldsymbol{P}(\boldsymbol{x}^*, p^*) - \mathbf{1})^{-1} \partial_p \boldsymbol{P}(\boldsymbol{x}^*, p^*), \tag{2.32}$$

i.e. $\boldsymbol{\xi}(p)$ corresponds to the intersection with $\mathcal{P}$ of the perturbed periodic trajectory for the parameter value $p \approx p^*$. Equivalently, it follows that there exists a curve of fixed points of $\boldsymbol{P}$ in the vicinity of $\boldsymbol{x}^*$ parametrized by p.

To overcome the singularity associated with an eigenvalue of $\partial_{\boldsymbol{x}}\boldsymbol{P}(\boldsymbol{x}^*, p^*)$ equal to 1, suppose that the matrix

$$\begin{pmatrix} \partial_{\boldsymbol{x}}\boldsymbol{P}(\boldsymbol{x}^*, p^*) - \mathbf{1} & \partial_p \boldsymbol{P}(\boldsymbol{x}^*, p^*) \end{pmatrix} \tag{2.33}$$

is rank n. Let $\begin{pmatrix} \boldsymbol{t} & \tau \end{pmatrix}^{\mathrm{T}}$ be a unit vector in the corresponding null space and introduce a function $\sigma(\boldsymbol{x}, p, \lambda)$, such that

$$\sigma(\boldsymbol{x}^*, p^*, 0) = 0, \quad \partial_{\boldsymbol{x}}\sigma(\boldsymbol{x}^*, p^*, 0) = \boldsymbol{t}^{\mathrm{T}} \quad \text{and} \quad \partial_p \sigma(\boldsymbol{x}^*, p^*, 0) = \tau. \tag{2.34}$$

Now consider the function

$$\boldsymbol{F}(\boldsymbol{x}, p, \lambda) = \begin{pmatrix} \boldsymbol{P}(\boldsymbol{x}, p) - \boldsymbol{x} \\ \sigma(\boldsymbol{x}, p, \lambda) \end{pmatrix}, \tag{2.35}$$

such that

$$\boldsymbol{F}(\boldsymbol{x}^*, p^*, 0) = \begin{pmatrix} \mathbf{0} \\ 0 \end{pmatrix}. \tag{2.36}$$

By assumption, the matrix

$$\begin{pmatrix} \partial_{\boldsymbol{x}}\boldsymbol{F}(\boldsymbol{x}^*, p^*, 0) & \partial_p \boldsymbol{F}(\boldsymbol{x}^*, p^*, 0) \end{pmatrix} = \begin{pmatrix} \partial_{\boldsymbol{x}}\boldsymbol{P}(\boldsymbol{x}^*, p^*) - \mathbf{1} & \partial_p \boldsymbol{P}(\boldsymbol{x}^*, p^*) \\ \boldsymbol{t}^{\mathrm{T}} & \tau \end{pmatrix}, \tag{2.37}$$

must be non-singular. The implicit function theorem again implies the existence of unique smooth functions $\boldsymbol{\xi}(\lambda)$ and $\pi(\lambda)$ for $\lambda \approx 0$, such that $\boldsymbol{\xi}(0) = \boldsymbol{x}^*$, $\pi(0) = p^*$,

$$\boldsymbol{F}(\boldsymbol{\xi}(\lambda), \pi(\lambda), \lambda) \equiv 0, \qquad \partial_\lambda \boldsymbol{\xi}(0) = \boldsymbol{t} \quad \text{and} \quad \partial_\lambda \pi(0) = \tau. \tag{2.38}$$

A Newton–Raphson-based algorithm that relies on this latter formulation forms the basis for the pseudo-arclength continuation scheme (cf. Nayfeh & Balachandran 1995) employed in later sections to map out the locus of periodic oscillations.

Remark 2.7. As an alternative to a Newton–Raphson-based algorithm, it is possible to formulate a feedback-based strategy that may be employed to continue a branch of periodic trajectories independently of their stability properties in the absence of control. Specifically, from remark 2.6 follows the existence of unique smooth functions $\boldsymbol{\xi}(\lambda)$ and $\pi(\lambda)$ for $\lambda \approx 0$, which describe a segment of a branch of fixed points corresponding to periodic trajectories of the original dynamical system, such that

$$\sigma(\boldsymbol{\xi}(\lambda), \pi(\lambda), \lambda) \equiv 0. \tag{2.39}$$

Introduce a smooth function $g(\boldsymbol{x}, p, q)$ for $\boldsymbol{x} \approx \boldsymbol{x}^*$, $p \approx p^*$ and $q \approx 0$, such that

$$g(\boldsymbol{x}^*, p^*, 0) = 0 \quad \text{and} \quad \partial_q g(\boldsymbol{x}^*, p^*, 0) \neq 0. \tag{2.40}$$

From an analysis similar to that in remark 2.6, it follows that there exists a unique smooth function $\rho(\lambda)$ for $\lambda \approx 0$, such that

$$g(\boldsymbol{\xi}(\lambda), \pi(\lambda), \rho(\lambda)) \equiv 0. \tag{2.41}$$

Now suppose that the feedback correction takes the form

$$\boldsymbol{g}_{\mathrm{control},\lambda} : \begin{pmatrix} \boldsymbol{x} \\ p \\ q \end{pmatrix} \mapsto \begin{pmatrix} \boldsymbol{x} \\ p + g(\boldsymbol{x}, p, q) \\ q + \sigma(\boldsymbol{x}, p, \lambda) \end{pmatrix}, \tag{2.42}$$

such that the Poincaré map for the controlled system is given by the composition $(\,\boldsymbol{P} \quad \boldsymbol{I} \quad \boldsymbol{I}\,)^{\mathrm{T}} \circ \boldsymbol{g}_{\mathrm{control},\lambda}$. Let $\delta\boldsymbol{x}=\boldsymbol{x}-\boldsymbol{\xi}(\lambda)$, $\delta p=p-\pi(\lambda)$ and $\delta q=q-\rho(\lambda)$. Taylor's theorem again implies

$$\begin{pmatrix} \delta\boldsymbol{x}^{(k+1)} \\ \delta p^{(k+1)} \\ \delta q^{(k+1)} \end{pmatrix} \approx (A + BK) \cdot \begin{pmatrix} \delta\boldsymbol{x}^{(k)} \\ \delta p^{(k)} \\ \delta q^{(k)} \end{pmatrix}, \tag{2.43}$$

where

$$\left.\begin{aligned} A &= \begin{pmatrix} \partial_{\boldsymbol{x}}\boldsymbol{P}(\boldsymbol{\xi}(\lambda), \pi(\lambda)) & \partial_p\boldsymbol{P}(\boldsymbol{\xi}(\lambda), \pi(\lambda)) & 0 \\ \boldsymbol{0} & 1 & 0 \\ \partial_{\boldsymbol{x}}\sigma(\boldsymbol{\xi}(\lambda), \pi(\lambda), \lambda) & \partial_p\sigma(\boldsymbol{\xi}(\lambda), \pi(\lambda), \lambda) & 1 \end{pmatrix}, \\ B &= \begin{pmatrix} \partial_p\boldsymbol{P}(\boldsymbol{\xi}(\lambda), \pi(\lambda)) \\ 1 \\ 0 \end{pmatrix}, \end{aligned}\right\} \tag{2.44}$$

and

$$K = \begin{pmatrix} \partial_{\boldsymbol{x}} g(\boldsymbol{\xi}(\lambda), \pi(\lambda), \rho(\lambda)) & \partial_p g(\boldsymbol{\xi}(\lambda), \pi(\lambda), \rho(\lambda)) & \partial_q g(\boldsymbol{\xi}(\lambda), \pi(\lambda), \rho(\lambda)) \end{pmatrix}$$

The controllability of the pair (A, B) is equivalent to the requirement that the matrix $(\,A-s\boldsymbol{1} \quad B\,)$ be rank $n+2$ for all eigenvalues s of A. For $\lambda\approx 0$, this is easily seen to follow from the non-singularity of the matrix

$$\begin{pmatrix} \partial_{\boldsymbol{x}}\boldsymbol{P}(\boldsymbol{x}^*, p^*) - \boldsymbol{1} & \partial_p\boldsymbol{P}(\boldsymbol{x}^*, p^*) \\ \boldsymbol{t}^{\mathrm{T}} & \tau \end{pmatrix} \tag{2.45}$$

considered above. Thus, for $\lambda\approx 0$, it is again possible to arbitrarily place the eigenvalues of $A+BK$.

Remark 2.8. As a special case of the discussion in remark 2.7, suppose that

$$\partial_p g(\boldsymbol{x}, p, q) = -1. \tag{2.46}$$

It follows that there exists a unique smooth function $\eta(\boldsymbol{x}, q)$ for $\boldsymbol{x}\approx\boldsymbol{\xi}(\lambda)$ and $q\approx\rho(\lambda)$, such that

$$\eta(\boldsymbol{\xi}(\lambda), \rho(\lambda)) = \pi(\lambda), g(\boldsymbol{x}, \eta(\boldsymbol{x}, q), q) \equiv 0, \tag{2.47}$$

$$\partial_{\boldsymbol{x}}\eta(\boldsymbol{\xi}(\lambda), \rho(\lambda)) = \partial_{\boldsymbol{x}} g(\boldsymbol{\xi}(\lambda), \pi(\lambda), \rho(\lambda)) \tag{2.48}$$

and

$$\partial_q\eta(\boldsymbol{\xi}(\lambda), \rho(\lambda)) = \partial_q g(\boldsymbol{\xi}(\lambda), \pi(\lambda), \rho(\lambda)). \tag{2.49}$$

Now consider the alternative formulation for the feedback correction (cf. Siettos & Kevrekidis 2004)

$$\boldsymbol{g}_{\mathrm{control},\lambda}\colon \begin{pmatrix} \boldsymbol{x} \\ p \\ q \end{pmatrix} \mapsto \begin{pmatrix} \boldsymbol{x} \\ \eta(\boldsymbol{x}, q) \\ q + \sigma(\boldsymbol{x}, \eta(\boldsymbol{x}, q), \lambda) \end{pmatrix}, \tag{2.50}$$

such that the Poincaré map for the controlled system is given by the composition $(\,\boldsymbol{P}\quad \boldsymbol{I}\quad \boldsymbol{I}\,)^{\mathrm{T}} \circ \boldsymbol{g}_{\mathrm{control},\lambda}$. Let $\delta\boldsymbol{x} = \boldsymbol{x} - \boldsymbol{\xi}(\lambda)$ and $\delta q = q - \rho(\lambda)$. Taylor's theorem again implies

$$\begin{pmatrix} \delta\boldsymbol{x}^{(k+1)} \\ \delta q^{(k+1)} \end{pmatrix} \approx (A + BK) \cdot \begin{pmatrix} \delta\boldsymbol{x}^{(k)} \\ \delta q^{(k)} \end{pmatrix}, \tag{2.51}$$

where

$$A = \begin{pmatrix} \partial_{\boldsymbol{x}}\boldsymbol{P}(\boldsymbol{\xi}(\lambda), \pi(\lambda)) & \boldsymbol{0} \\ \partial_{\boldsymbol{x}}\sigma(\boldsymbol{\xi}(\lambda), \pi(\lambda), \lambda) & 1 \end{pmatrix}, \qquad B = \begin{pmatrix} \partial_p \boldsymbol{P}(\boldsymbol{\xi}(\lambda), \pi(\lambda)) \\ \partial_p \sigma(\boldsymbol{\xi}(\lambda), \pi(\lambda), \lambda) \end{pmatrix} \tag{2.52}$$

and

$$K = \begin{pmatrix} \partial_{\boldsymbol{x}} g(\boldsymbol{\xi}(\lambda), \pi(\lambda), \rho(\lambda)) & \partial_q g(\boldsymbol{\xi}(\lambda), \pi(\lambda), \rho(\lambda)) \end{pmatrix}. \tag{2.53}$$

The controllability of the pair (A, B) is equivalent to the requirement that the matrix $(\,A - s\boldsymbol{1}\quad B\,)$ be rank $n+1$ for all eigenvalues of s of A. For $\lambda \approx 0$, this is again easily seen to follow from the non-singularity of the matrix

$$\begin{pmatrix} \partial_{\boldsymbol{x}}\boldsymbol{P}(\boldsymbol{x}^*, p^*) - \boldsymbol{1} & \partial_p \boldsymbol{P}(\boldsymbol{x}^*, p^*) \\ \boldsymbol{t}^{\mathrm{T}} & \tau \end{pmatrix} \tag{2.54}$$

considered above. Thus, for $\lambda \approx 0$, it is again possible to arbitrarily place the eigenvalues of $A + BK$.

Remark 2.9. Denote by A the coefficient matrix governing the linearized dynamics (cf. equation (2.7)). In the absence of modelling error and noise, A may be computed by the procedure outlined in remark 2.4. To enable a robust (and possibly adaptive and real-time) estimation of A in the presence of modelling uncertainty or noisy data, consider the quadratic function

$$V(A) = \frac{1}{2} \sum_{k=1}^{N-1} \left\| \delta\boldsymbol{x}^{(k)} - A\delta\boldsymbol{x}^{(k-1)} \right\|^2, \tag{2.55}$$

given a set of N data points $\delta\boldsymbol{x}^{(k)}$, $k = 0, \ldots, N-1$. The *least-squares estimate* of the matrix A is given by the *global minimizer* of the function V. Denote by $\partial_A V$ the matrix of partial derivatives of V with respect to the entries of its matrix argument. Then, the least-squares estimate is the unique matrix for which $\partial_A V$ equals the zero matrix and can be computed directly from the given data.

3. Applications to tapping-mode AFMs

(*a*) *Modelling and phenomenology*

The dynamics of the AFM probe tip in traditional tapping-mode operation may be described by a lumped-parameter model in which the spatial shape of the vibrating beam is approximated by the first fundamental mode of vibration of

the beam (Yagasaki 2004). Denote by x and $\dot{x}$ the displacement of the probe tip relative to some reference level and the tip speed, respectively, in the direction perpendicular to the sample surface, such that $\dot{x} > 0$ corresponds to the motion of the tip towards the sample surface. Let ω denote the angular frequency of the sinusoidal excitation of the dither piezo that controls the position of the cantilever support. In terms of the *state vector*

$$\boldsymbol{x} = (\, x \quad \dot{x} \quad \theta \,)^{\mathrm{T}} \in \mathbb{R}^2 \times \mathbb{S}^1, \tag{3.1}$$

where $\theta = \omega t \bmod 2\pi$, the vector field may be written as

$$\boldsymbol{f}(\boldsymbol{x}) = \left(\dot{x} \quad -2\xi\omega_0\dot{x} - \omega_0^2 x - a_{\mathrm{ts}}(x + s, \dot{x}) + \gamma \cos\theta \quad \omega \right)^{\mathrm{T}}, \tag{3.2}$$

where ω_0 is the natural frequency of the first fundamental mode of the cantilever; ξ is the damping ratio capturing any internal dissipation in the cantilever and possible damping due to the motion in the ambient environment; a_{ts} is the contribution to the tip acceleration from the tip–sample interactions; s characterizes the equilibrium separation between the cantilever support and the onset of repulsive interactions between the probe tip and the sample surface; and γ is the amplitude of the contribution to the tip acceleration from the dither excitation.

A variety of models of the tip–sample interactions have been reported in the literature. Here, two separate force field models are considered, namely the piecewise-linear model

$$a_{\mathrm{ts}}(x, \dot{x}) = \begin{cases} 0, & d \le x, \\ -\alpha(x - d), & 0 \le x < d\,, \\ -\alpha(x - d) + \beta x + c_\beta \dot{x}, & x < 0, \end{cases} \tag{3.3}$$

introduced by Sebastian *et al.* (2001) and the piecewise-nonlinear model

$$a_{\mathrm{ts}}(x, \dot{x}) = \begin{cases} \alpha(x + d)^{-2}, & 0 \le x, \\ \alpha d^{-2} - \beta |x|^{3/2}, & x < 0, \end{cases} \tag{3.4}$$

discussed, for example, by Yagasaki (2004). Here, the positive numbers α and β represent the strengths of the attractive and repulsive force components, respectively; d represents the effective distance from the sample surface beyond which the attractive forces become negligible in the piecewise-linear model; c_β models additional dissipative effects due to 'contact' in the piecewise-linear model; and αd^{-2} represents the adhesive force during contact in the piecewise-nonlinear model (table 1).

For fixed values of excitation amplitude and excitation frequency, variations in the equilibrium separation s result in changes in the number and linearized stability properties of different steady-state responses of the probe tip (see García & San Paulo 2000; Lee *et al.* 2002; San Paulo & García 2002). For large values of s, the probe-tip response is sinusoidal with angular frequency equal to ω and amplitude and phase lag directly related to the system parameters through formulae obtainable from a purely linear analysis, neglecting the influence of a_{ts}. Moreover, as reported in the literature, for certain ranges of excitation amplitude and frequency, there exist ranges of values of the equilibrium separation in which three periodic steady-state oscillations coexist. Of these, one corresponds to oscillations of the probe tip that remain bounded away from the onset of the

Table 1. Numerical values of the parameters in the piecewise-linear (from Sebastian *et al.* 2001) and piecewise-nonlinear (from Yagasaki 2004) tip–sample interaction force models.

parameter	piecewise-linear	piecewise-nonlinear
ξ	0.0038	0.0150
ω_0	4.642×10^5 rad s^{-1}	2.7646×10^5 rad s^{-1}
ω	4.642×10^5 rad s^{-1}	2.8500×10^5 rad s^{-1}
α	9.5895×10^{10} s^{-2}	4.2122×10^{-17} Nm^2 kg^{-1}
β	9.1811×10^{12} s^{-2}	1.1612×10^{17} N(m s^{-1})$^{-(3/2)}$ kg^{-1}
c_β	7.8073×10^{10} s^{-1}	
d	1.695×10^{-9} m	0.38×10^{-9} m
γ	39.305 m s^{-2}	150 m s^{-2}

repulsive interactions, referred to here as *non-contacting oscillation*. The other two correspond to oscillations of the probe tip that penetrate past the onset of repulsive interactions referred to here as *contacting oscillations*. Indeed, it has been found (García & San Paulo 2000) that even small amounts of noise may suffice to induce transitions between coexisting stable steady-state oscillations. Such phenomena are observed using a variety of more or less realistic tip–sample interaction force models that combine a weak long-range attractive force with a strong short-range repulsive force field (see García & San Paulo 2000; Lee *et al.* 2002; San Paulo & García 2002).

Figure 1 shows branches of non-contacting and contacting periodic oscillations obtained through model-based continuation (cf. remark 2.6) for each of the two tip–sample interaction force models. Here, it can be seen that, in representative parameter regions, the non-contacting oscillations are asymptotically stable, whereas one of the contacting oscillations is asymptotically stable and the other is unstable. The branches of contacting and non-contacting oscillations come together at critical bifurcation points known as saddle-node bifurcations, which are denoted by 'SN' in figure 1.

(*b*) *Feedback control*

Feedback control is used in conjunction with tapping-mode AFMs in order to maintain a desired response amplitude of the cantilever oscillations and, indirectly, to extract information during surface scanning of the sample profile. In particular, given a set point for the response amplitude, it is assumed that the changes in the equilibrium separation s between the cantilever and the sample required to achieve this control objective correspond directly to changes in the surface topography. In the event, however, that there exist two (or more) asymptotically stable (in the presence of control) steady-state oscillatory responses with identical amplitude but distinct values of s, this assumption is no longer valid. Moreover, after an initial transient, the cantilever response may settle on any one of these oscillations, thus corrupting imaging performance of the AFM system. In the case that the post-transient behaviour is a contacting oscillation with a significant contact velocity and duration, this may result in damage to softer sample surfaces.

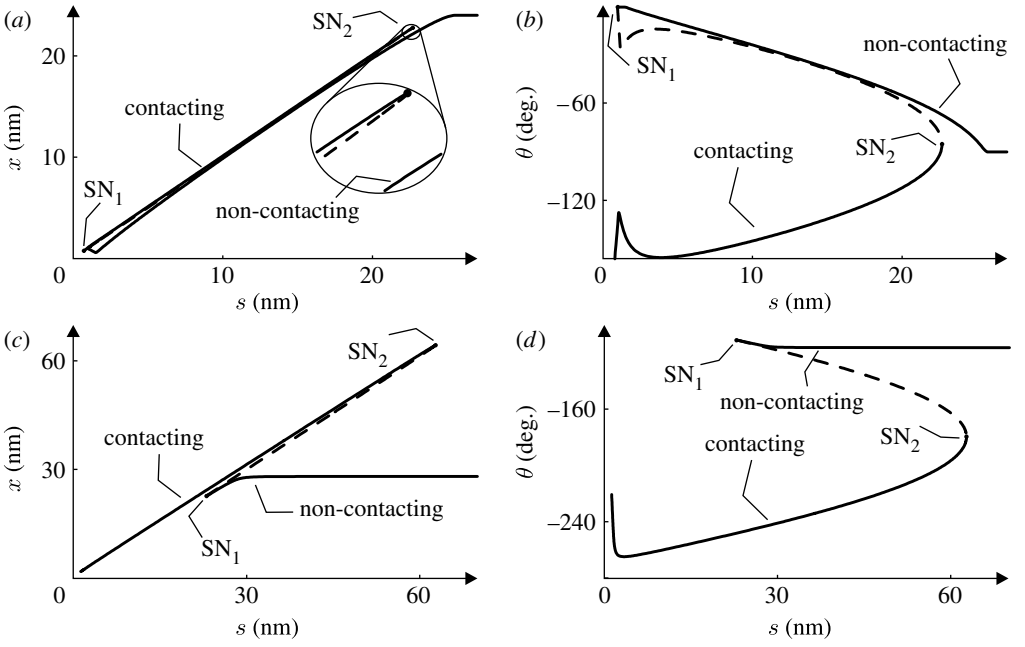

Figure 1. Changes in the maximum deviation between the cantilever tip and the sample surface and in the corresponding phase lag under changes in the equilibrium separation distance for (*a*,*b*) the piecewise-linear and (*c*,*d*) the piecewise-nonlinear force models. Dashed lines indicate unstable oscillations, while solid lines indicate stable oscillations. The corresponding branches of periodic solutions are connected through two saddle-node bifurcation points at SN_1 and SN_2.

Whereas oscillations with identical response amplitude may be found for different values of s, as suggested in figure 1, their *phase shift* (defined, for example, as the value of θ at the moment when the maximum displacement of the cantilever tip away from the surface is achieved) may be used to distinguish between different values of s. The phase shift is already used in existing AFM systems to quantify changes in surface properties other than topography. The confluence of changes in topography and material properties in actual measurements, however, would be expected to render the distinction between amplitude and phase shift information artificial.

In this paper, we propose using sampled measurements of the phase shift θ and the cantilever displacement x and the imposition of event-driven control as discussed previously for the purposes of

— enabling a clearer distinction between non-contacting and contacting oscillations and preventing undesired transitions between different branches of non-contacting and contacting oscillations for the purposes of improved imaging,
— stabilization of the branch of (in the absence of control) unstable contacting oscillations for the purposes of achieving tapping-mode operation with lower contact velocities, reduced duration of contact, but with a negligible decrease in oscillation amplitude when compared with the branch of asymptotically stable contacting oscillations, and
— increasing the speed of surface scanning by decreasing the duration of transient dynamics.

As suggested previously, significant changes in the local stability properties of periodic oscillations may be achieved through the purposeful design of the linearized properties of the feedback control map. Through the design of nonlinear properties of the control map, it may subsequently be possible to make changes to nonlinear stability characteristics, such as sizes and shapes of basins of attraction, although this will not be explicitly undertaken here.

In the notation introduced in the discussion of the OGY control strategy, let the equilibrium separation s take the role of the system parameter p and suppose that $\mathcal{P}$ is the zero-level surface of the function $h_{\mathcal{P}}(\boldsymbol{x}) = \dot{x}$. The control strategy imposes changes in the equilibrium separation so as to change the linearized stability characteristics of desirable steady-state cantilever oscillations even in the presence of noise and uncertainty (cf. remark 2.9). Although our primary concern is with the case that the actual value of s is not measurable (after all, the purpose of the control strategy is to indirectly compute this value), we will consider the cases of the full-state, partial-state and estimated-state feedback strategies in the numerical results presented in §4.

4. Numerical results

(*a*) *Estimation of the linearized dynamics*

Suppose that the locations of the fixed points of the Poincaré map are known for a given value of the equilibrium separation. Then, following remark 2.9, least-squares estimation may be used to robustly estimate the sensitivity matrix A in equation (2.7) directly from experimental time-series data. This allows one to overcome inaccuracies in the theoretical predictions due to modelling assumptions and uncertainties in system parameters and may allow for real-time adaptation of feedback parameters in the case of parameter drift or changes in material properties of the sample.

For illustrative purposes, we estimate the A matrix for both the tip–sample contact models and compare the estimated results with those obtained from the direct method discussed in remark 2.4. We consider an equilibrium separation of 15 nm for the piecewise-linear model and 26.2 nm for the piecewise-nonlinear model. The corresponding values for maximum tip displacement away from the sample surface and phase shift for the stable non-contacting, stable contacting and unstable contacting oscillations are given in tables 2 and 3.

Example estimates of the A matrix obtained by least-squares approximation based on the time-series data from 20 cycles of the excitation are shown in table 4 for the stable non-contacting and unstable contacting oscillations found in the piecewise-nonlinear tip–sample model (with comparable results for the other oscillations). The predictions from the estimation process match closely those obtained from the direct method not only for stable periodic oscillations, but also for the unstable periodic oscillations with typical relative errors of the order of a few per cent. The only cases where the relative error of estimation exceeds 5% are for elements of the A matrix whose absolute values are significantly smaller than those of the other elements. Clearly, the accuracy of the estimation procedure is a function of N. While longer datasets may be expected to lead to better estimates, care must be taken in the case of unstable oscillations to ensure that the deviations from the corresponding fixed points remain small.

Table 2. Three possible solutions at a separation of 15 nm for the piecewise-linear tip–sample force model.

type of solution	amplitude (in nm)	phase (in rad)
stable non-contacting	14.9015	2.4695
unstable contacting	14.9708	2.4595
stable contacting	15.1066	0.8748

Table 3. Three possible solutions at a separation of 26.2 nm for the piecewise-nonlinear tip–sample force model.

type of solution	amplitude (in nm)	phase (in rad)
stable non-contacting	25.4378	2.7276
unstable contacting	26.0255	2.7176
stable contacting	27.5493	0.4399

Table 4. Numerical comparison between the predicted values for the non-trivial entries of the A matrix and its eigenvalues computed using the method in remark 2.4 and those estimated using the method in remark 2.9 for the stable non-contacting (columns 2 and 3) and the unstable contacting (columns 4 and 5) oscillations, respectively, found in the piecewise-nonlinear tip–sample model at $s=26.2$ nm.

parameter	prediction	estimate	prediction	estimate
$\boldsymbol{a}_{11}$	1.4291	1.4276	0.3969	0.4023
$\boldsymbol{a}_{12}$	−6.5338	−6.5304	3.6093	3.6096
$\boldsymbol{a}_{13}$	−0.5661	−0.5650	0.5525	0.5475
$\boldsymbol{a}_{21}$	−0.1864	−0.1860	−0.1836	−0.1830
$\boldsymbol{a}_{22}$	1.4350	1.4341	0.4286	0.4416
$\boldsymbol{a}_{23}$	0.2033	0.2029	0.1973	0.1970
λ_1	0.3284	0.3286	0.4128+0.8138i	0.4219+0.8125i
λ_2	2.5357	2.5329	0.4128−0.8138i	0.4219−0.8125i

(*b*) *Experimental detection of unstable oscillations*

From the model-based bifurcation diagrams (figure 1), the existence of unstable periodic oscillations is well established for the tapping-mode cantilever dynamics. While it is possible to use feedback control to stabilize an unstable periodic oscillation, locating the unstable periodic oscillation branch experimentally is challenging (to say the very least) due to the diverging nature of the local dynamics. Furthermore, using the theoretically obtained unstable periodic oscillations as reference for feedback-based control is error prone, for example, due to uncertainties involving tip–sample contact model fidelity, parameter creep and noise in electronic circuitry. A possible solution for locating an unstable periodic oscillation, even in the presence of such exogenous disturbances, would be

to mimic the continuation process of remark 2.6 in an experimental paradigm as described in remarks 2.7 and 2.8. The implementation of such a scheme in the form of an algorithm is presented below.

— *Step 1.* Initiate the algorithm with a known periodic oscillation $(\boldsymbol{x}^*, p^*)$ (e.g. a stable non-contacting oscillation that can be easily found for large values of s) and estimate the corresponding $\partial_{\boldsymbol{x}}\boldsymbol{P}(\boldsymbol{x}^*, p^*)$ and $\partial_p\boldsymbol{P}(\boldsymbol{x}^*, p^*)$ matrices following the method in remark 2.9. Use these to estimate $\boldsymbol{t}$ and τ.
— *Step 2.* Consider the feedback strategy in remark 2.8, where

$$g(\boldsymbol{x}, p, q) = p^* - p + \boldsymbol{k}_1^{\mathrm{T}} \cdot (\boldsymbol{x} - \boldsymbol{x}^*) + k_2 q \tag{4.1}$$

and

$$\sigma(\boldsymbol{x}, p, \lambda) = \boldsymbol{t}^{\mathrm{T}} \cdot (\boldsymbol{x} - \boldsymbol{x}^*) + \tau(p - p^*) - \lambda. \tag{4.2}$$

In particular, it follows that

$$\eta(\boldsymbol{x}, q) = p^* + \boldsymbol{k}_1^{\mathrm{T}} \cdot (\boldsymbol{x} - \boldsymbol{x}^*) + k_2 q \tag{4.3}$$

and thus

$$\sigma(\boldsymbol{x}, \eta(\boldsymbol{x}, q), \lambda) = \left(\boldsymbol{t}^{\mathrm{T}} + \tau \boldsymbol{k}_1^{\mathrm{T}}\right) \cdot (\boldsymbol{x} - \boldsymbol{x}^*) + \tau k_2 q - \lambda. \tag{4.4}$$

Formulate the full-state feedback gains so as to place the eigenvalues of the closed-loop system given in equation (2.51) with $\lambda = 0$ at any arbitrary desired location inside the unit circle.
— *Step 3.* Estimate an initial guess for the fixed point with a non-zero λ as per the formulae

$$\boldsymbol{x}_0 = \boldsymbol{x}^* + \boldsymbol{t}\lambda \quad \text{and} \quad q_0 = \frac{\tau - \boldsymbol{k}_1^{\mathrm{T}} \cdot \boldsymbol{t}}{k_2} \lambda. \tag{4.5}$$

— *Step 4.* Allow the controlled dynamics to converge to a new periodic oscillation by iterating the map equation (2.51). Relabel the corresponding fixed point as $\boldsymbol{x}^*$ (where $p^* = \eta(\boldsymbol{x}^*, q^*)$) and repeat from step 1.

The above algorithm was used to generate the bifurcation diagrams shown in figure 2. It compares very favourably with the bifurcation diagram obtained using the conventional model-based continuation scheme. Here, an adaptive algorithm was used to promote large values of λ in step 3 in as far as the dynamics in step 4 would converge, and to repeat step 3 with a smaller λ in the case of no convergence. In a practical implementation, this adaptive algorithm would need to be replaced by a fixed-step algorithm, with a step size determined by the magnitude of the curvature of the bifurcation curve near the upper saddle-node bifurcation.

We note that the results in figure 2 involve two separate runs, starting at a stable contacting oscillation and a stable non-contacting oscillation for large s. Of these, only the former run succeeded in turning around at the corresponding saddle-node point to enable locating unstable contacting oscillations. By contrast, as documented in previous work by Dankowicz (2006), Zhao & Dankowicz (2006) and Dankowicz *et al.* (2007), the rates of change of the entries of the Jacobian of the Poincaré map near the lower saddle-node point are very large (indeed, in the two models considered here, it grows beyond all bounds as the periodic oscillation

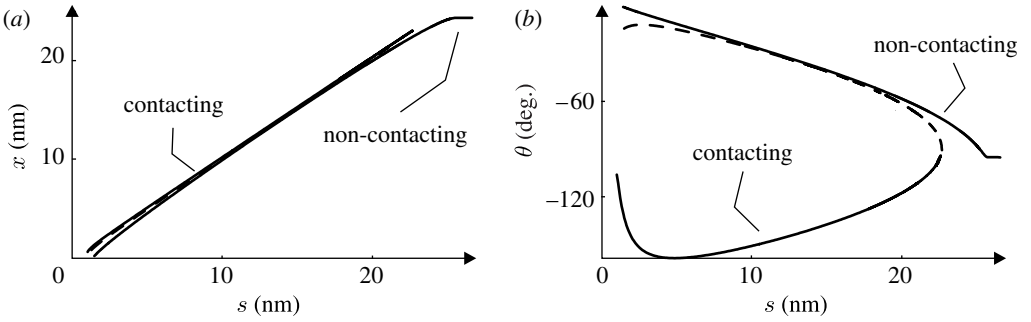

Figure 2. (*a*,*b*) Bifurcation diagram obtained through feedback control-based approach for the piecewise-linear tip–sample force model. Solid lines represent stable periodic oscillations, while dashed lines represent unstable periodic oscillations. Here, the values of $\boldsymbol{k}_1$ and k_2 were chosen so as to ensure a placement of the eigenvalues of the closed-loop system (2.51) at 0.75, 0.85 and 0.9.

approaches grazing contact with the state-space discontinuity corresponding to the onset of repulsive force interactions). The ability to achieve convergence in step 4 using the feedback gains from step 2 is thus severely diminished and the maximum value of λ becomes impractically small.

(*c*) *Feedback stabilization*

After establishing methodologies for estimating the sensitivity matrix and locating the unstable periodic oscillations using time-series data, we proceed to demonstrate the efficacy of the proposed control strategies in achieving the objectives of stabilizing the unstable periodic oscillations as well as reducing the extent of transient dynamics in the vicinity of stable periodic oscillations. Numerical values for the entries of the K matrix that achieve a given choice of eigenvalues of the closed-loop system in the case of the full-state feedback are listed in table 5 for the stable non-contacting, unstable contacting and stable contacting oscillation states from table 2.

Figure 3 shows the result of applying the full-state feedback strategy to the unstable periodic oscillation in the presence of small noise-induced perturbations in the state vector. Whereas the dynamics quickly diverge from the original periodic oscillation in the absence of control, the full-state feedback strategy successfully stabilizes the periodic oscillation. From figure 3*b*, it is clear that by stabilizing the unstable oscillation, surface imaging may be achieved with a lower impact velocity than would result from relying on the high-amplitude stable contacting oscillations.

The full-state feedback strategy is not useful for imaging purposes as the parameter corresponding to equilibrium separation s is not available as an output. In fact, the purpose of applying control is to indirectly estimate the instantaneous separation between the cantilever base and the sample being imaged. Following the analysis in previous sections, we consider two alternate strategies, namely partial-state feedback and estimated-state feedback. Although the partial-state feedback does not allow for arbitrary eigenvalue placement, for the given dynamical system, a search of gain parameters revealed that it is nevertheless possible to stabilize the periodic oscillation by a suitable choice of gain parameters (table 6).

Table 5. The values of the entries of the full-state feedback gain matrix K corresponding to eigenvalues of the coefficient matrix of the closed-loop system inside the unit circle at 0.2, 0.25 and 0.3 for the piecewise-linear tip–sample force model at $s=15$ nm for the three different oscillations listed in table 2.

type of solution	K_1	K_2	K_3
stable non-contacting	30.13	−35.16	0.98
unstable contacting	−5.44	10.63	0.98
stable contacting	2.38	−2.41	0.97

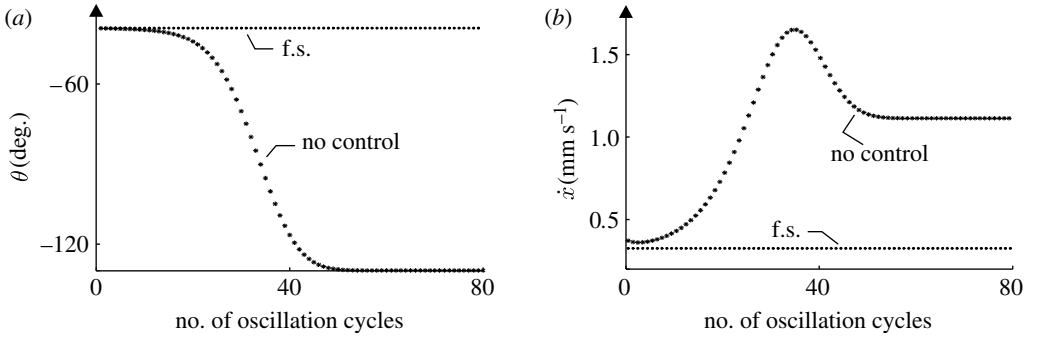

Figure 3. Successive values of (a) the oscillation phase lag and (b) impact velocity in the absence of control using the full-state (f.s.) feedback strategy for a trajectory based at an initial condition very close to an unstable periodic oscillation in the piecewise-linear tip–sample interaction model.

Table 6. Values of the partial-state feedback gain matrix K corresponding to eigenvalues of the coefficient matrix of the closed-loop system inside the unit circle for the piecewise-linear tip–sample force model at $s=15$ nm for the three different periodic oscillations listed in table 2.

type of solution	K_1	K_2	K_3
stable non-contacting	−0.02	−0.26	0
unstable contacting	−0.02	−0.5	0
stable contacting	−0.83	0.16	0

Figure 4 shows the result of applying the three feedback strategies with appropriately chosen gain parameters to a slightly perturbed initial condition away from the desired periodic oscillation. It is observed that the full-state and estimated-state feedback strategies both result in faster convergence to the periodic oscillation than does the partial-state feedback strategy.

(*d*) *Surface scanning*

Now consider the scan stability of the proposed feedback control schemes, i.e. of their ability to maintain a desired periodic oscillation while scanning the sample surface at fairly high lateral speeds. It is desirable in the practical operation of the AFM to achieve fast convergence to the desired set-point

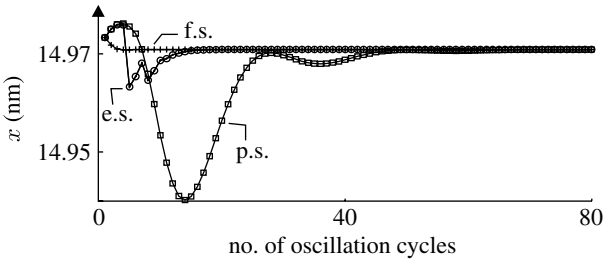

Figure 4. Comparison between the convergence properties of the full-state (f.s.), estimated-state (e.s.) and partial-state (p.s.) feedback approaches near an unstable periodic oscillation in the piecewise-linear tip–sample interaction model.

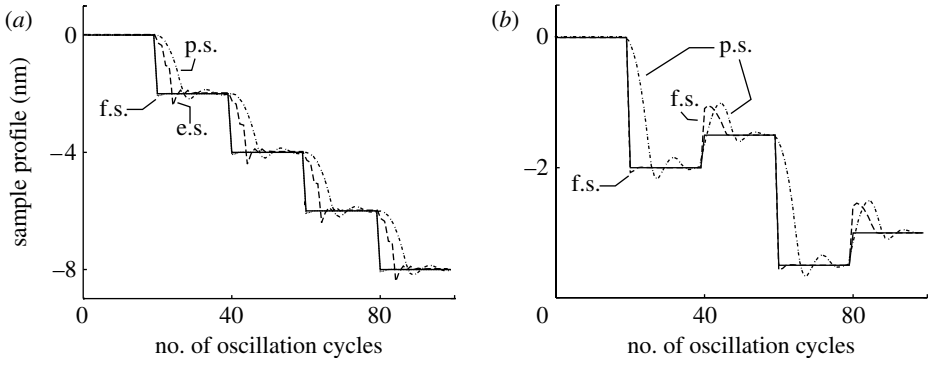

Figure 5. Tracking performance of the proposed full-state (f.s.), estimated-state (e.s.) and partial-state (p.s.) feedback strategies while following (*a*) a decreasing stepped sample profile and (*b*) an alternatingly decreasing and increasing sample profile for a stable contacting periodic oscillation in the piecewise-linear tip–sample interaction model. The fast convergence (less than five oscillation cycles) of the full-state feedback in (*a*) results in close agreement with the stepped sample profile. In (*b*) estimated-state feedback (not shown) was not able to track the desired profile.

separation while responding to the surface topography variations. Too high a scan rate, however, may potentially destabilize the dynamics by not allowing the controller to converge to the set point before the arrival of a new disturbance input. Here, the proposed control strategies are examined in regard to their ability to maintain the stability of the periodic oscillation under the influence of a train of disturbance inputs in the form of surface profile variations.

Figure 5 shows the tracking performance of the full-state, partial-state and estimated-state feedback strategies during scanning of a decreasing and an alternatingly increasing and decreasing stepped profile, respectively. Here, discrete changes in the lateral placement of the cantilever are imposed every 0.2707 ms, i.e. every 20 oscillation cycles of the cantilever. We can observe from figure 5 that application of the full-state feedback strategy provides very good tracking (convergence in less than five oscillation cycles). The partial-state feedback strategy seems reasonably effective in tracking, though with a slower convergence rate (approx. 20 oscillation cycles) than the full-state feedback strategy. The convergence rates of the different control strategies differ between

decreasing and increasing sample height variations (e.g. less than five and greater than ten oscillation cycles, respectively, for the full-state feedback strategy). This effect is found to be particularly severe for the estimated-state feedback strategy.

5. Conclusions

This paper has documented a variety of dynamical systems-based, control-theoretic analytical, computational and experimental tools for investigating and exploiting the natural oscillating dynamics of the cantilever in tapping-mode operation of AFMs. While the feedback strategies discussed here have previously appeared in the literature in various guises, the present discussion collects this using a self-consistent notation and clearly demonstrates their applicability to the AFM dynamics. In particular, the numerical results have demonstrated the possibility of

— stabilizing periodic oscillations independently of their stability characteristics in the absence of control. Indeed, although the analysis above is only local (given its foundation in a linearized analysis), convergence to a desired periodic oscillation has been found, even for quite large perturbations in initial conditions;
— experimentally estimating the sensitivity matrix describing the dynamics in the vicinity of a desired periodic oscillation;
— maintaining a low-impact velocity during tapping-mode operation by applying the feedback strategies in the vicinity of an originally unstable periodic contacting oscillation when compared with that obtained for a stable contacting oscillation;
— increasing the lateral surface scan rate through the reduction of the duration of transient dynamics near a desired periodic oscillation and without encountering the hysteretic effects usually observed while approaching or withdrawing from the surface during imaging; and
— experimentally mapping out the bifurcation structure of the AFM dynamics in a manner similar to that of generating a dynamic force curve as carried out during AFM calibration. This would allow, for example, for the possibility of experimentally observing the location of saddle-node bifurcation points in the force–distance curve and to experimentally investigate their change in location as a consequence of variation in excitation amplitude, frequency, sample surface and parameter creep. This has so far only been possible in simulation-based analysis.

The implementation of the (linear) control schemes outlined here is straightforward in principle, but would naturally be accompanied by a variety of application-specific challenges in an experimental set-up. Nevertheless, as the analysis has shown, a successful implementation affords the possibility of significantly improved AFM operation. It would be very valuable to attempt such an implementation and to evaluate its possible benefits to lateral scan rates, sample integrity and repeatability of imaging. The adaptive estimation scheme also affords a means to compensate for time-dependent model uncertainties, such as noise and creep effects. From a control-theoretic viewpoint, it would also be interesting to formulate real-time optimization schemes for choosing the numerical values of the gain matrix K, as well as higher order derivatives of the control and observer functions.

This material is based upon work supported by the National Science Foundation under grant no. 0619028. Our thanks also to Dr Craig Prater of Veeco, Inc. for his insight and helpful suggestions.

References

Andreivskii, B. R. & Fradkov, A. L. 2003 Control of chaos: methods & applications. *Autom. Remote Control* **64**, 673–713. (doi:10.1023/A:1023684619933)

Ashhab, M., Salapaka, M. V., Dahleh M. & Mezic I. 1997 Control of chaos in atomic force microscopes. In *Proc. of the American Control Conf., Albuquerque, New Mexico, June 1997.*

Chen, C. T. 1999 *Linear system theory and design.* Oxford, UK: Oxford University Press.

Dankowicz, H. 2006 Nonlinear dynamics as an essential tool for nondestructive characterization of soft nanostructures using tapping mode atomic force microscopy. *Phil. Trans. R. Soc. A* **364**, 3505–3520. (doi:10.1098/rsta.2006.1907)

Dankowicz, H., Zhao, X. & Misra, S. 2007 Near-grazing dynamics in tapping-mode atomic force microscopy. *Int. J. Non-Linear Mech.* **42**, 697–709. (doi:10.1016/j.ijnonlinmec.2006.10.005)

García, R. & San Paulo, A. 2000 Dynamics of a vibrating tip near or in intermittent contact with a surface. *Phys. Rev. B* **61**, R13 381–R13 384. (doi:10.1103/PhysRevB.61.R13381)

Jamitzky, F., Stark, M., Bunk, W., Heckl, W. M. & Stark, R. W. 2006 Chaos in dynamic atomic force microscopy. *Nanotechnology* **17**, S213–S220. (doi:10.1088/0957-4484/17/7/S19)

Lee, S. I., Howell, S. W., Raman, A. & Reifenberger, R. 2002 Nonlinear dynamics of micro cantilevers in tapping mode atomic force microscopy: a comparison between theory and experiment. *Phys. Rev. B* **66**, 115 409. (doi:10.1103/PhysRevB.66.115409)

Nayfeh, A. H. & Balachandran, B. 1995 *Applied nonlinear dynamics.* Wiley series in nonlinear science. New York, NY: Wiley.

Ott, E., Grebogi, C. & Yorke, J. A. 1990 Controlling chaos. *Phys. Rev. Lett.* **64**, 1196–1199. (doi:10.1103/PhysRevLett.64.1196)

San Paulo, A. & García, R. 2002 Unifying theory of tapping-mode atomic-force microscopy. *Phys. Rev. B* **66**, 041 406. (doi:10.1103/PhysRevB.66.041406)

Sebastian, A., Salapaka, M. V., Chen, D. J. & Cleveland, J. P. 2001 Harmonic and power balance tools for tapping-mode atomic force microscope. *J. Appl. Phys.* **89**, 6473–6480. (doi:10.1063/1.1365440)

Siettos, C. I. & Kevrekidis, I. G. 2004 Coarse bifurcation diagrams via microscopic simulators: a state feedback approach. *Int. J. Bifurcation Chaos* **14**, 207–220. (doi:10.1142/S0218127404009193)

Stark, R. W. 2005 Time delay Q-control of the microcantilever in dynamic atomic force microscopy. In *Proc. of 2005 5th IEEE Conf. on Nanotechnology, Nagoya, Japan, July 2005.* (doi:10.1109/NANO.2005.1500745)

Syrmos, V. L., Abdallah, C. T., Dorato, P. & Grigoriadis, K. 1997 Static output feedback—a survey. *Automatica* **33**, 125–137. (doi:10.1016/S0005-1098(96)00141-0)

Uchihashi, T., Kodera, N., Itoh, H., Yamashita, H. & Ando, T. 2006 Feed-forward compensation for high-speed atomic force microscopy imaging of biomolecules. *Jpn J. Appl. Phys.* **45**, 1904–1908. (doi:10.1143/JJAP.45.1904)

Yagasaki, K. 2004 Nonlinear dynamics of vibrating micro cantilevers in tapping-mode atomic force microscopy. *Phys. Rev. B* **70**, 245 419. (doi:10.1103/PhysRevB.70.245419)

Yamasue, K. & Hikihara, T. 2006 Control of microcantilevers in dynamic force microscopy using time delayed feedback. *Rev. Sci. Instrum.* **77**, 053 703. (doi:10.1063/1.2200747)

Zhao, X. & Dankowicz, H. 2006 Characterization of intermittent contact in tapping-mode atomic force microscopy. *J. Comput. Nonlinear Dynam.-Trans. ASME* **1**, 109–115. (doi:10.1115/1.2162864)